ACS SENSORS

pubs.acs.org/acssensors

Article

Persistent Luminescence Nanosensors: A Generalized Optode-Based Platform for Autofluorescence-Free Sensing in Biological Systems

Tyler Z. Sodia, Hanna L. Tetu, Samuel C. Saccomano, Elizabeth G. Letch, John M. Branning, Jr., Adrian A. Mendonsa, Shubham Vyas, and Kevin J. Cash*

Cite This: *ACS Sens.* 2024, 9, 3307−3315

Read Online

ACCESS | Metrics & More | Article Recommendations | Supporting Information

ABSTRACT: Fluorescent nanosensors have revolutionized diagnostics and our ability to monitor cellular dynamics. Yet, distinguishing sensor signals from autofluorescence remains a challenge. Here, we merged optode-based sensing with near-infrared-emitting $ZnGa_2O_4:Cr^{3+}$ persistent luminescence nanoparticles (PLNPs) to create nanocomposites for autofluorescence-free "glow-in-the-dark" sensing. Hydrophobic modification and incorporation of the persistent luminescence nanoparticles into an optode-based nanoparticle core yielded persistent luminescence nanosensors (PLNs) for five analytes (K^+, Na^+, Ca^{2+}, pH, and O_2) via two distinct mechanisms. We demonstrated the viability of the PLNs by quantifying K^+ in fetal bovine serum, calibrating the pH PLNs in the same, and ratiometrically monitoring O_2 metabolism in cultures of *Saccharomyces cerevisiae*, all the while overcoming their respective autofluorescence signatures. This highly modular platform allows for facile tuning of the sensing functionality, optical properties, and surface chemistry and promises high signal-to-noise ratios in complex optical environments.

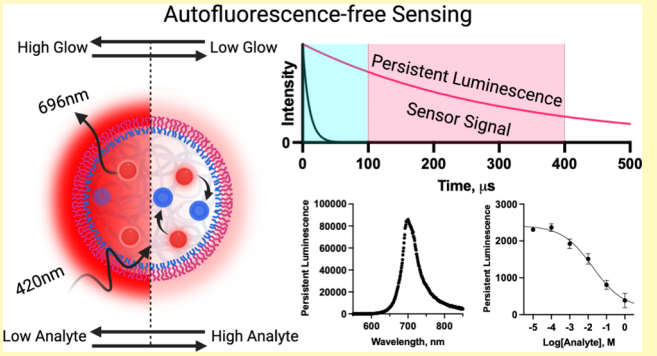

KEYWORDS: *persistent luminescence, ionophore, nanosensor, optode, nanocomposite, chemosensor, oxygen sensing*

Nanoparticle-based optical sensors are invaluable tools for investigating chemical and biological systems.[1−3] Persistent luminescence nanoparticles (PLNPs) are gaining prominence as they mitigate interference from native fluorescent molecules, enabling precise optical sensing.[4−6] Unlike traditional methods that rely on wavelength separation, PLNPs offer temporal signal distinction through their prolonged emission, circumventing autofluorescence interference from the sample.[7−9] Functionalizing the PLNP surface has enabled autofluorescence-free sensing of proteins, nucleic acids, and small biomolecules.[10−13]

Another noteworthy category of nanosensors originates from polymeric optode membranes that function on target analyte partitioning and its interactions with chemical moieties in the particle's hydrophobic core.[14] This two-phase architecture allows for the facile switching of components to sense different analytes or adjust optical properties.[14−16] Importantly, it facilitates the integration of luminescent nanomaterials into the sensor matrix, such as CdSe/ZnS core−shell quantum dots,[17] upconversion $NaYF_4$:Er,Yb nanorods,[18] silicon nanocrystals,[19] and graphene carbon dots.[20,21] In 2019, our team devised a Na^+-selective optode membrane integrating a persistent luminescence microparticle.[22] However, the size of the luminescent particles prevented the fabrication of nanosensors, constraining both the response time and applicability in numerous systems.

Here, we combined optode-based sensing with persistent luminescence nanoparticles to create functional nanocomposites that we term persistent luminescence nanosensors (PLNs). Through flash nanoprecipitation (FNP), we integrated hydrophobically modified chromium-doped zinc gallate ($ZGO:Cr^{3+}$) PLNPs into polymer nanoparticles for autofluorescence-free signal acquisition and quantification. We demonstrate two sensing schemes utilizing $ZGO:Cr^{3+}$. First, a traditional ionophore-based approach[14] couples selective ion extraction and the variable absorption of a lipophilic pH indicator to the persistent luminescence of $ZGO:Cr^{3+}$, enabling the detection of K^+, Na^+, Ca^{2+}, or pH (Scheme 1A). The second scheme enables ratiometric, time-resolved O_2 sensing by utilizing $ZGO:Cr^{3+}$ persistent luminescence as an internal standard signal alongside the O_2-sensitive phosphorescence emission of palladium-TPTBP (Scheme 1B). Employing a

Received: March 21, 2024
Revised: May 2, 2024
Accepted: May 17, 2024
Published: June 3, 2024

https://doi.org/10.1021/acssensors.4c00653
ACS Sens. 2024, 9, 3307−3315

Scheme 1. Sensing Mechanisms[a]

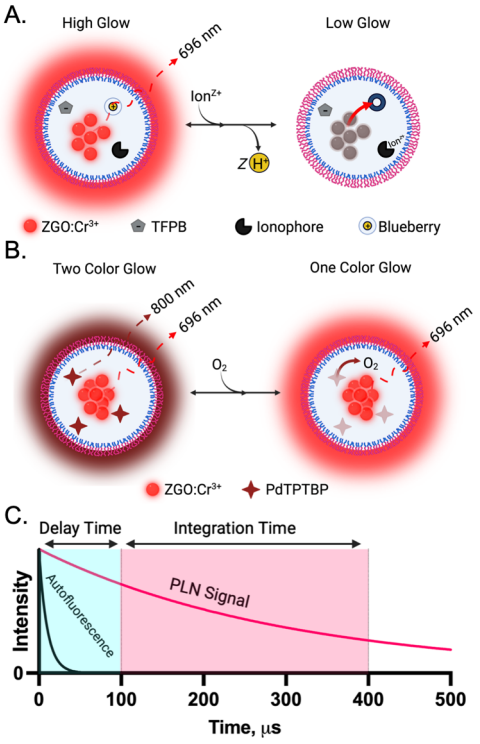

[a](A) Ion-selective PLN mechanism: ions in the surrounding bulk phase displace a proton from the pH-sensitive blueberry dye, increasing its absorbance which gates the persistent luminescence of ZGO:Cr^{3+}. (B) O_2 PLN mechanism: a ratiometric readout where PdTPTBP is dynamically quenched by O_2, while ZGO:Cr^{3+} is unaffected by O_2. (C) Approach for time-resolved luminescence detection with PLNs.

time-resolved approach (Scheme 1C) allows for the exclusion of autofluorescence from biological samples, enabling direct measurement of sensor signals, despite significant spectral overlap.

EXPERIMENTAL SECTION

Materials. Tetrahydrofuran (THF), dimethylformamide (DMF), sodium tetrakis-[3,5-bis(trifluoromethyl)phenyl]borate (NaTFPB; Selectophore), bis(ethylhexyl) sebecate (BEHS), sodium ionophore X (Selectophore), potassium ionophore I (Selectophore), calcium ionophore II (Selectophore), chromoionophore II (ChII; Selectophore), 4-(2-hydroxyethyl)piperazine-1-ethanesulfonic acid (HEPES), tris(hydroxymethyl)aminomethane (TRIS), Dulbecco's phosphate-buffered saline (PBS), boric acid, sodium phosphate monobasic, sodium citrate, trimethoxy(octyl)silane (TMOS), sodium chloride, potassium chloride, calcium chloride, magnesium chloride, zinc nitrate hexahydrate, gallium nitrate hydrate, chromium nitrate nonahydrate, and polycaprolactone-*b*-poly(ethylene oxide)(COOH) were all purchased from Sigma-Aldrich. Blueberry-C6-ester-652 was purchased from Biosearch Technologies (Genomic Analysis by LGC). Fetal bovine serum (FBS) was obtained from Thermo Fisher. Yeast (Kolsch I) and fast pitch wort were purchased from Tom's Brew shop in Lakewood, CO. Polystyrene-*b*-poly(ethylene oxide) (PS-*b*-PEO) and polystyrene-*b*-poly(acrylic acid) (PS-*b*-PAA) were purchased from Polymer Source, Inc. Palladium tetraphenyl tetrabenzoporphine (PdTPTBP) was obtained from Frontier Specialty Chemicals.

Methods. *ZGO:Cr Synthesis.* Raw ZGO:Cr PLNPs ($ZnGa_2O_4$:Cr^{3+}, 0.4% Cr^{3+}/Ga^{3+}) were synthesized according to methods reported by Li et al. with some modifications.[23] 594.98 mg of $Zn(NO_3)_2{\cdot}6H_2O$, 547.52 mg of $Ga(NO_3)_3{\cdot}H_2O$, and 3.2 mg of $Cr(NO_3)_3{\cdot}9H_2O$ were dissolved in 15 mL of Milli-Q H_2O and titrated to pH 9 with concentrated NH_4OH (28%). This cloudy solution was vigorously stirred for 1 h and then transferred to a 30 mL PTFE-lined hydrothermal reactor and placed in an oven at 220° C for 10 h. The reactor was allowed to cool naturally to room temperature. The precipitate was centrifuged at 3500 rpm for 5 min and then washed thrice with 1 N HCl to remove the ZnO adsorbed to the surface of the product. After washing, the white product was placed in an oven at 60° C for 24 h to dry.

ZGO:Cr Surface Modification. To modify the surface of raw ZGO:Cr, the dried product was dispersed in ultrapure DMF (10 mg/mL) and transferred to a round-bottom flask. Trimethoxy(octyl)silane (TMOS) was added (150 μL of TMOS/100 mg of raw ZGO:Cr) directly to the flask and vigorously stirred at 80°C for 20 h to obtain a white precipitate. The precipitate was centrifuged at 3500 rpm for 5 min and washed thrice with DMF to remove any unreacted TMOS. After the last centrifugation, ZGO:Cr@TMOS was dispersed in THF at 40 mg/mL in a glass vial with a PTFE-lined cap and stored at 20° C in the dark.

ZGO:Cr Characterization. Powder X-ray diffractometry was done with a Scintag XDS-2000 (Cu Kα1 = 1.5406 Å). The transmission electron micrograph of raw ZGO:Cr^{3+} was obtained with a FEI Co. Talos F200X 200 keV field-emission scanning/transmission electron microscope (Figure 1C). Fourier transform infrared (FT-IR) spectroscopy was done on a Nicolet Summit FT-IR spectrometer (iD1 Transmission, Thermo Scientific) to confirm surface functionalization with trimethoxy(octyl)silane.

Luminescence Lifetime Measurements. To achieve the two excitation wavelengths used (420 and 266 nm), two different beamlines were employed, both using a Surelite III Q-switched Nd:YAG nanosecond laser as the pump source. The path that generated the 266 nm beam included the Surelite III with the second harmonic installed (generating 532 nm light), which was converted to 266 nm using an external fourth harmonic crystal. The 420 nm beam was generated using the Surelite III with both the second and third harmonics installed (generating 355 nm light) in tandem with a Horizon optical parametric oscillator (OPO). The output power in the sample chamber for each wavelength was ~20 and ~15 mJ for 266 and 420 nm, respectively. The luminescence at 696 nm was measured for all samples (with backgrounds subtracted). Decay curves were plotted and fit in GraphPad Prism and then normalized to the maximum value. Lifetimes were calculated from the resulting parameters (see eq S1).

Nanocomposite Synthesis and Characterization. All nanocomposite ZGO:Cr@TMOS was made by flash nanoprecipitation using a confined-impingement jet (CIJ) mixer. To synthesize the nanocomposites without any optode-based sensing components, 15 mg of ZGO:Cr@TMOS (40 mg/mL) was mixed with 125 μL of the block-*co*-polymer, PS-*b*-PEO (20 mg/mL) for a total of 500 μL. This mixture was transferred to a 1 mL syringe as the solvent stream for FNP (see Figure 2C). The antisolvent was composed of 525 μL of phosphate-buffered saline (pH 7.4). The two streams were rapidly mixed in the CIJ mixer into a quench bath of 5 mL of PBS.

The ion PLNs were made similarly. All solvent streams for the ion PLNs contained 10 mg of ZGO:Cr@TMOS, 10 mg of Ps-*b*-PEO, and the necessary optode-based sensing components in 500 μL of THF. For K^+ PLNs, 0.5 mg of blueberry, 1 mg of Na^+TFPB^-, 1.5 mg of K^+ ionophore I, and 2 mg of BEHS (2.2 μL) were added to the solvent stream mixture. The solvent stream for Na^+ PLNs contained the same components as those of the K^+ PLNs, but K^+ ionophore I was replaced by Na^+ ionophore X (component masses were kept constant). The solvent stream of Ca^{2+} PLNs had 1.5 mg of Ca^{2+} ionophore II, 1 mg of Na^+TFPB^-, 0.5 mg of blueberry, and 2 mg of BEHS (2.2 μL). Each solvent stream was precipitated against a HEPES/Tris antisolvent stream (525 μL) with a CIJ mixer into a 5 mL quench bath of HEPES/Tris. THF was then evaporated with compressed air for 20 min, and the PLNs were filtered with a 0.8 μm PES filter into a glass vial and stored in the dark.

The pH PLNs were made similarly to the nanocomposites. Briefly, 15 mg of ZGO:Cr@TMOS (40 mg/mL) was mixed with 125 μL of

https://doi.org/10.1021/acssensors.4c00653
ACS Sens. 2024, 9, 3307−3315

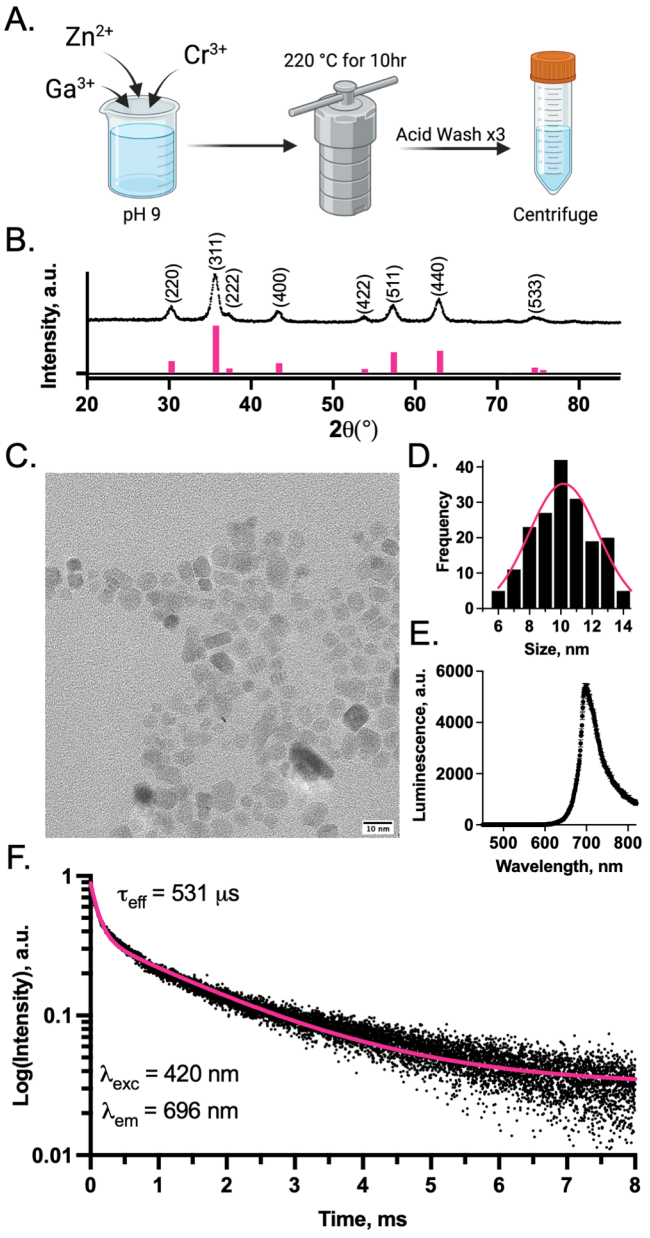

Figure 1. PLNP Characterization. (A) Schematic of hydrothermal synthesis and processing. (B) X-ray diffraction pattern showing a pure cubic spinel structure (ICDD = 00-038-1240). (C) HR-TEM image of ZGO:Cr^{3+} (scale bar = 10 nm). (D) Frequency size distribution of ZGO:Cr^{3+} PLNPs (obtained from 200 particles). (E) Luminescence spectrum of ZGO:Cr^{3+} after 420 nm excitation. (F) Luminescence decay of ZGO:Cr^{3+} after 420 nm pulse excitation.

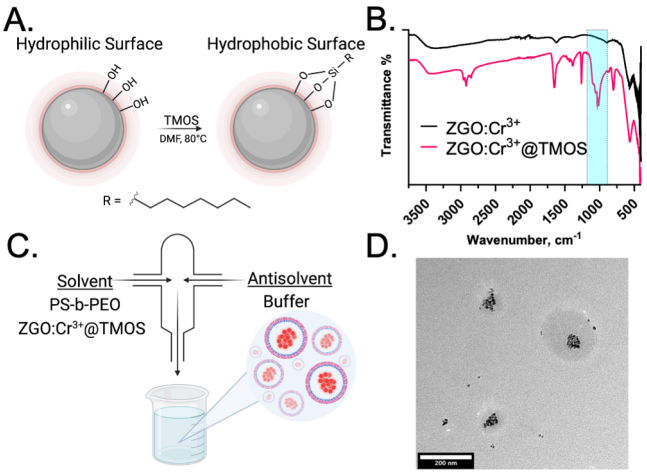

Figure 2. Surface modification of ZGO:Cr^{3+} NPs and their incorporation into a polymeric nanoparticle. (A) Schematic of silane attachment. (B) FT-IR spectrograph highlighting siloxane attachment to the PLNP surface. (C) Schematic of the principle of flash nanoprecipitation for nanocomposite fabrication. (D) TEM image of the ZGO:Cr^{3+}@TMOS@PS-*b*-PEO nanocomposite.

the block-*co*-polymer PS-*b*-PEO (20 mg/mL) for a total of 500 μL. Chromoionophore II (0.04 mg, 6 mg/mL) was added to this mixture before being transferred to a 1 mL syringe as the solvent stream for FNP. The antisolvent and quench bath for the pH PLNs was deionized water. The K^+ PLNs with ChII were fabricated similarly to the pH PLNs—0.5 mg of NaBARF and 0.5 K^+ ionophore I were added to the solvent stream with other particle components.

All ion PLNs were calibrated against K^+, Na^+, Ca^{2+}, and Mg^{2+} (10 nM to 1 M) with a separate solution method (1:1 v/v). The pH PLNs were calibrated in Britton–Robinson buffer and "saline-spiked" Britton–Robinson buffer that contained 154 mM NaCl, 5 mM KCl, 8 mM $MgCl_2$, and 2.4 mM $CaCl_2$. Both buffers had a subset of standards with the pH range 3–9. The ion PLN and pH PLN calibrations were done in a Nunc MicroWell 96-well optical bottom plate (Nalgene Nunc International). All luminescence measurements were taken with a BioTek Synergy H1 hybrid multimode microplate reader with a red-shifted PMT (Winooski, VT). All time-gated luminescence measurements were taken on the plate reader's time-resolved fluorescence setting. The functional lifetime of the ion and pH PLNs were obtained by calibrating the sensors to their respective analyte on days 0, 4, and 8. The reversibility of the K^+ PLNs was tested using a similar procedure as previous work.[16,24] Briefly, the K^+ PLNs were concentrated to 10×, put into a hollow fiber microdialysis tube (MWCO, 13 kDa; Spectrum Laboratories), sealed at each end, and then secured onto a microscope slide with vacuum grease. Quickly, the tube was submerged in HEPES/Tris buffer (pH 7.4), and the initial reading (no K^+) was taken on an Olympus Fluoview FV10i-W laser scanning confocal microscope (ex: 405; em: 700). The buffer was removed, and the slide was gently rinsed before the addition of 100 μL of 1 M KCl. After 20 min incubation, another image was taken with the same settings. This cycle was repeated twice in triplicate.

To make the O_2 PLNs, the chromoionophore in the pH PLNs was replaced with 5 μg of palladium tetraphenyl tetrabenzoporphine (PdTPTBP). The antisolvent and quench bath for the O_2 PLNs was PBS. The O_2 PLNs were calibrated similarly as our previous works.[25] Before calibration, the O_2 PLNs were concentrated to 3× using a 10 kDa Amicon centrifugation filter. Then, 1.5 mL of 3× O_2 PLNs was used in a septum-sealed quartz cuvette with a 2 mm path length and fitted with a gas line and a vent using 22 gauge needles. Gas flow rates from an air and nitrogen tank were controlled with mass flow controllers and mixed in a 25 mL mixing chamber to form gas streams with various concentrations of O_2 from 0 to 21% atm (or 0 to 6.65 mg/L) dissolved O_2 at an elevation of 5780 ft (Golden, CO). The gas was bubbled into the cuvette at a total flow rate of 3 mL/min, and the O_2 concentration was confirmed with an O_2 electrode fit for piercing (UniSense, Denmark). To obtain the luminescence intensities, the cuvette was placed in a custom 3D-printed microplate fit for a septum-sealed cuvette and then analyzed with the same plate reader as the ion PLNs. The sample was excited with the plate reader's flash xenon lamp, and emission was read at 696 nm (ZGO:Cr^{3+}) and 800 nm (PdTPTBP). Steady-state luminescence intensities and time-gated luminescence intensities (TG = 100 or 250 μs) with a 1 ms integration time were used for Stern–Volmer and pseudo-Stern–Volmer plots.

The size and ζ-potential of all nanocomposites (PLNs included) were measured on a Brookhaven ZetaPALS instrument (Brookhaven Instruments Corporation, Holtsville, NY). The transmission electron

https://doi.org/10.1021/acssensors.4c00653
ACS Sens. 2024, 9, 3307–3315

micrographs of all PLNs were recorded with a Tecnai G2 Spirit TWIN (T12, 20−120 kV) (Figures 2D and S6).

Fetal Bovine Serum Analysis. To show that the persistent luminescence signal from ZGO:Cr^{3+} could overcome FBS autofluorescence, the ZGO:Cr^{3+}@TMOS@Ps-*b*-PEO nanocomposite was mixed 1:1 with stock FBS in a 96-well optical bottom plate. Steady-state and time-gated (100 μs) luminescence spectra were obtained in the aforementioned plate reader setup.

FBS was then adjusted to pH 3−9 with either 1 N NaOH or 1 N HCl and mixed 1:1 with pH PLNs. The raw, delayed luminescence signal (100, 250, 500 μs, or 1 ms) was compared to the saline-spiked Britton−Robinson buffered standards, and both were adjusted to omit any inner filter effects using eq S2.

We measured the K^+ concentration in FBS with a similar procedure. The stock FBS was mixed with K^+ PLNs in a 1:1 v/v ratio (n = 8). The raw time-resolved luminescence (100 μs delay) was IFE-adjusted using eq S2 and compared to the IFE-adjusted standard K^+ calibration curve.

Yeast Assay. The O_2 metabolism of yeast was monitored with the O_2 PLNs according to established methods.[25−27] First, the O_2 PLNs were concentrated to 10× stock with a 10 kDa Amicon centrifugation filter and set aside. *Saccharomyces cerevisiae* (Kolsch I) was diluted in filtered PBS at 1:10 and 1:100 stock concentrations. The wort media for yeast growth was decanted and filtered through a 0.22 μm PES vacuum filter. Next, 20 μL of yeast dilutions, 130 μL of filtered wort, and 50 μL of 10× O_2 PLNs were pipetted into a 96-well optical bottom plate, each dilution having 8 replicates. We included control wells in the octuplet that excluded either yeast or O_2 PLNs. The samples were incubated at 30 °C and shaken for 2 min before each reading, with readings taken every 15 min over a 60 h period. At 42 h, 20 μL of concentrated PMB was added to 4 of the 8 replicates, and 20 μL of PBS was added to the other 4 replicates. An aluminum foil plate cover was used to cover the 96-well plate with minute holes punched into the foil for PMB or PBS addition at 42 h. A schematic of the plate setup is shown in Figure S21.

All statistical analysis and plotting were done in GraphPad Prism (v. 10.1). All visual schematics were created with BioRender.

RESULTS AND DISCUSSION

We synthesized ZGO:Cr^{3+} hydrothermally to produce cubic-phase nanocrystals measuring 10 ± 2 nm in diameter, as shown in Figure 1A−D, with a ζ-potential of 34 ± 1.1 mV, facilitating easy dispersion in water. The luminescence spectrum in Figure 1E, centered at 696 nm, corresponds to the spin-forbidden $^2E \rightarrow {}^4A_2$ transition of Cr^{3+}.[5] The ZGO:Cr^{3+} NPs exhibit three excitation bands at 254, 420, and 580 nm, representing d−d transitions of Cr^{3+} (Figure S1).[5] Upon pulse excitation at 420 nm, the Cr^{3+} emission peak displayed multiexponential decay, with an effective luminescence lifetime (τ_{eff}) of 531 μs using eq S1. The luminescence decay at 696 nm extends into the millisecond range following both 420 nm (Figure 1F) and 266 nm (Figure S2) pulse excitations, deeming ZGO:Cr^{3+} ready for the next steps toward integration into our optode-based persistent luminescence-sensing approach.

In many biological applications, modifications are necessary to attach recognition sites and/or stabilizing agents to the ZGO:Cr^{3+} surface for sensing or improved aqueous stability.[4,5,28] However, our ZGO:Cr^{3+} PLNPs require a hydrophobic surface to be retained in the organic phase of the optode-based nanosensor. We achieved this by modifying raw ZGO:Cr^{3+} NPs through condensation of trimethoxy-(octyl)silane onto their hydroxide surface, yielding ZGO:Cr^{3+}@TMOS (Figure 2A), which remains stable in nonpolar environments like the optode matrix. Fourier transform infrared (FT-IR) spectroscopy confirmed the successful condensation, with characteristic peaks indicating Si−O−Si stretching (1090, 1053, 1033, and 1015 cm^{-1}) and C(sp^3)-H bonds (2958, 2923, and 2855 cm^{-1}) of the octyl silane attachment protruding from the particle surface (Figure 2B).

Flash nanoprecipitation (FNP) is a nanoparticle fabrication technique capable of encapsulating various materials within polymer nanoparticles.[29] Using FNP, we created persistent luminescence nanocomposites comprising ZGO:Cr^{3+}@TMOS and polystyrene-*b*-poly(ethylene) oxide (PS-*b*-PEO), as illustrated in Figure 2C,D. These nanocomposites feature a hydrophobic core consisting of a blend of ZGO:Cr^{3+}@TMOS and PS, while the PEO coating ensures aqueous stability. However, other block copolymers are suitable for the fabrication of nanocomposites with different surface chemistries (Table S1). Before incorporating sensing components, we demonstrated that ZGO:Cr^{3+}@TMOS@PS-*b*-PEO effectively eliminates autofluorescence from fetal bovine serum (FBS) (Figure S3). FBS exhibits strong autofluorescence, peaking at 500 nm, which overlaps with the ZGO:Cr^{3+} emission, unless a time-resolved acquisition is used.

The optode sensor design revolves around selecting functional components within a hydrophobic polymer matrix. The ionophore, serving as the recognition unit, extracts and stabilizes the desired ion within the nanoparticle core. Simultaneously, the nonfluorescent pH indicator, blueberry-C6-ester-652 (blueberry), undergoes deprotonation, leading to increased absorbance and modulation of PLNP emission. An ionic additive, Na^+TFPB^-, was introduced into the sensor core to neutralize the positive charge on protonated blueberry. By combining blueberry and Na^+TFPB^- with potassium ionophore I, sodium ionophore X, or calcium ionophore II in the FNP solvent stream, we generated K^+, Na^+, or Ca^{2+} PLNs, respectively. The emission from ion PLNs decreased with increasing analyte concentration and blueberry absorbance (Figures 3A−C and S4). The inclusion of optode components still allowed for the integration of ZGO:Cr^{3+}@TMOS into the PLN core, as illustrated in Figure S5. Notably, a comparison of micrographs between the PLNs (Figure S5) and nanocomposites lacking sensing components (Figure 2D) revealed potential variability in the distribution of ZGO:Cr^{3+}@TMOS within the composite particles. In the absence of sensing components, the PLNPs seem to aggregate in the core, whereas in the presence of optode components the PLNPs seem to relocate closer to the surface. This apparent variability may stem from factors such as the introduction of a plasticizer into the core, other additional mass from sensing components impacting precipitation kinetics during the FNP process, or disparities in PLNP surface functionalization across batches. Nevertheless, the sensing capability and the prolonged luminescence lifetime of the system remain consistent, irrespective of the apparent differences in the PLNP distribution within the nanocomposite.

With a 100 μs delay time, the K^+ PLNs in Figure 3A are 100 times more selective for K^+ over Na^+ ($\log K_{K,Na} = -2.1$) and possess a dynamic range that covers concentrations found in serum.[30] Notably, the response of K^+ PLNs remains consistent as the delay time extends to 1 ms, potentially enabling K^+ quantification in systems with fluorescent sources of variable luminescence lifetimes (e.g., in multiplexing scenarios) (Figure S6). Additionally, the K^+ PLNs demonstrate reversibility, supporting the anticipated equilibrium-based ion-exchange mechanism, and maintain functionality for at least 8 days (Figure S7 and S8).

https://doi.org/10.1021/acssensors.4c00653
ACS Sens. 2024, 9, 3307−3315

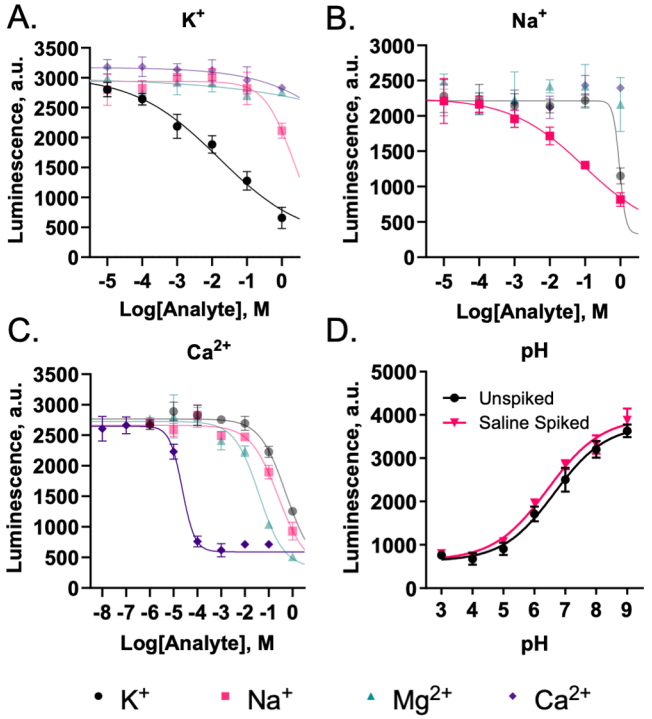

Figure 3. Calibration curves for the ion and pH persistent luminescence nanosensors. K^+ (A), Na^+ (B), and Ca^{2+} (C) sensors were tested against common ions in separate solutions, and all showed good selectivity (the target ion is darker in each panel). (D) pH PLN calibrations in Britton–Robinson universal buffer with (pink) or without (black) saline spike (n = 3 for all calibrations).

Similarly, using a 100 μs delay, the Na^+ PLNs depicted in Figure 3B exhibit a selectivity coefficient comparable to other Na^+ sensors utilizing the same ionophore and PEG-based surfactants ($\log K_{Na,K} = -1.1$).[31] The Na^+ PLNs have a dynamic range adequate for serum quantification and a functional lifespan ranging between 4 and 8 days (Figure S9). The Ca^{2+} PLNs (Figure 3C, 100 μs delay) are approximately 1000-fold more selective over the major competing ion Mg^{2+} ($\log K_{Ca,Mg} = -3.2$) and have a functional lifespan of less than 4 days (Figure S10). Detailed size and selectivity coefficient data for all ion PLNs are provided in Tables S1 and S2, respectively. To validate the ion-exchange mechanism of the ion PLNs, formulations excluding ionophores were tested for their time-resolved responses to ions. As anticipated, in the absence of an ionophore, the sensors respond according to ion lipophilicity (Hofmeister series) (Figure S11). Moreover, the exclusion of optode components from the formulation results in no response to pH or ions, indicating that the modulation of ZGO:Cr^{3+} emission depends on the dye's protonation degree and selective extraction (Figure S12).

Investigations into the functional lifetime of optode-based sensors have been a recurrent focus since their inception. A key factor influencing sensor lifetime is the potential leaching of either the plasticizer or the active sensing components dissolved within the optode matrix.[32,33] Given that the sole distinction among the ion PLN formulation lies in the ionophore, the observed variability in their functional lifetime (K: x > 8 days, Na: 8 days > x > 4 days, Ca: x < 4 days) may arise from fluctuations in the respective ionophore leaching kinetics or disparities in ionophore interactions with other sensing components inside the nanocomposite core.

Adjusting the PLN formulation to incorporate a different lipophilic pH indicator, chromoionophore II (ChII, ETH 2439), allowed us to measure across the biological pH range with persistent luminescence format (Figure 3D, 500 μs delay). The inverse relationship between pH and ChII absorbance at 700 nm (Figure S13) results in an increase in the ZGO:Cr^{3+} signal, as seen in Figure 3D. Importantly, the pH PLN response remains the same with multiple delay times (Figure S14) and when saline concentrations of ions are spiked into the buffered standards, indicating no significant response to ionic strength (Figure 3D, pink). The pH PLN signal was also tested against Na^+ and K^+ (10 μM–1 M)—no change in signal occurred (Figure S15). Additionally, the calibrations of pH PLNs were found to be consistent for 8 days (Figure S16). Next, the pH PLN response was measured in pH-adjusted FBS from pH 3 to 9. An inner filter effect (IFE) impacted the sensor signal but can be adjusted using established methods (see eq S2).[34] Using a delay time, we can omit FBS autofluorescence, achieving a signal-to-noise ratio of 120:1, and calibrate the pH PLNs in the serum while obtaining the same fit parameters as the response in buffered standards (Figure S17). Without a delay time, these measurements are not possible in FBS as the background signal is at least 5 times that of the sensor response (Figure S18).

Next, we utilized K^+ PLNs to measure K^+ in FBS. Upon mixing FBS with K^+ PLNs (1:1 v/v) and correcting for IFE, the K^+ concentration was determined to be 1.9 ± 0.8 mM. These findings underscore the potential of ion-selective PLNs for assessing real clinical samples, including those exhibiting background autofluorescence.

In 2015, Clark's group showed that blueberry-C6-ester-652 (blueberry) can replace the commonly used chromoionophores as a nonluminescent quencher dye and engage in selective ion exchange.[35] In their system, the high molar absorptivity of blueberry coupled with a static fluorophore resulted in a brighter and more selective nanosensor for K^+ compared to the nanosensor with chromoionophore III as the transducer. We chose to use the same approach for the K^+, Na^+, and Ca^{2+} PLNs to simplify our luminescence measurements (as blueberry is nonemissive) and due to the extensive overlap between the absorbance of deprotonated blueberry (~680 nm) and the persistent luminescence of ZGO:Cr^{3+} (696 nm). However, as demonstrated with pH PLNs, pH-sensitive transducers other than blueberry can be used to modulate the persistent luminescence of the PLNP. To explore this further, we developed a K^+ PLN utilizing ChII as the PLNP modulator, showing an increasing, time-resolved response as a function of K^+ (Figure S19). We speculate that a similar sensing mechanism would also be possible with oxazinoindolines[36] or solvatochromic transducers[37,38] if the variable absorbance of the indicator overlaps with the luminescence of the PLNP.

To fabricate O_2-sensitive PLNs, we used the phosphorescent PdTPTBP (em: 800 nm; τ_0 = 356 μs[39]) as the O_2 indicator and the ZGO:Cr^{3+} emission as the O_2-insensitive reference (Figure S20) for time-resolved, ratiometric measurements. Exciting the Pd-chelate results in an electronic transition to S_1 and intersystem crossing to an excited triplet state (T_1) causing spin inversion and a forbidden transition back to S_0—the mechanism of phosphorescence.[39,40] Molecular O_2 can collide with the dye and quench it, resulting in a lower emission

https://doi.org/10.1021/acssensors.4c00653
ACS Sens. 2024, 9, 3307–3315

intensity and a lower luminescence lifetime.[39,40] This collisional quenching process is typically characterized by the Stern−Volmer relationship (eq S3A). Ratiometric O_2 measurements can be described by a pseudo-Stern−Volmer relationship (eq S3B) by instead plotting the quotient of the ratiometric signal (PdTPTBP/ZGO:Cr^{3+}) at 0 mg/L O_2 by the same ratio at prevailing [O_2], giving a linear response (Figure 4A).[25,41] As expected, the pseudo-K_{sv} increases over the measured O_2 range by increasing the delay time—a function of the variable luminescence lifetime of PdTPTBP (Figures 4A and S21). The quenching mechanism of the indicator results in a diminished intensity and a diminished luminescence lifetime with increasing O_2. When implementing a delay time, the difference in the indicators' intensity at variable O_2 conditions is exaggerated compared to those at the steady state due to the disproportionate exclusion of emitted photons from indicators in higher O_2 conditions with shorter lifetimes. As a result, there is a system-specific limit to which the delay time can be increased without compromising the sensor's dynamic range. An example of this is shown in Figure 4B, where the calibrations with longer delay times have a smaller dynamic range but a higher sensitivity at low concentrations.

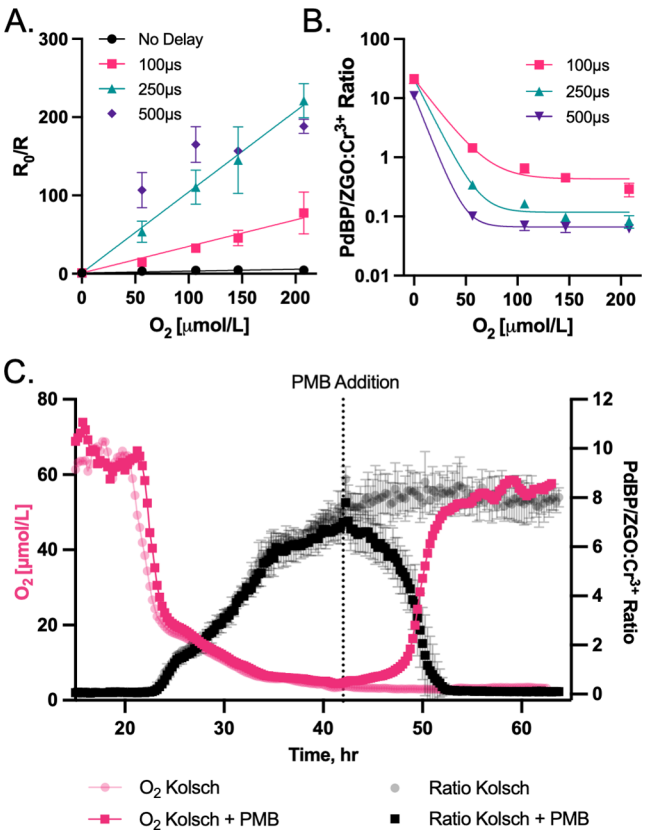

Figure 4. (A) Ratiometric calibration curves of the O_2 PLNs with various delay times fit to eq S3B (K_{psv} = 0.236, 3.35, and 10.2 for no delay, 100, and 250 μs, respectively). It was not useful to fit the data from the 500 μs delay. (B) PdTPTBP (PdBP)/ZGO:Cr^{3+} ratio as a function of O_2 on a semilog plot with an exponential fit. The dynamic range shrinks as a function of increasing delay time, but the sensitivity is increased within that range. (C) O_2 PLNs can track the O_2 metabolism of yeast over 60 h of incubation with a 500 μs delay time. The left y-axis shows the [O_2] in μmol/L (red and pink). Values shown are smoothed using a 2nd order polynomial with a 4-neighbor average. Unsmoothed data are shown in Figure S22. The right y-axis shows the ratiometric signal (black and gray). Pink and gray measurements show yeast cultures without the addition of potassium metabisulfite.

While spectral separation approaches have been used to overcome autofluorescence in microbial systems,[25,27,42,43] this work achieves this with ratiometric sensors that are compatible with a time-resolved measurement approach. O_2 consumption of *S. cerevisiae* (Kolsch I) was monitored over 65 h with the O_2 PLNs (plate setup in Figure S22). Using the obtained ratiometric signals from the yeast assay and the exponential fit to the data shown in Figure 4B, we can calculate the O_2 concentration inside the yeast cultures (see eq S4 and the associated fit parameters). Without a delay, yeast autofluorescence interferes with the ZGO:Cr^{3+} emission and precludes ratiometric O_2 measurements (Figures S23A and S24A), but using a 500 μs delay eliminates the autofluorescence and shows an increasing ratiometric signal at ∼20 h correlating to a drop in O_2 below 60 μmol/L (Figures 4C, S23B, and S24B). Before ∼20 h, the O_2 concentration in the culture exceeds the dynamic range of the O_2 PLN when using a 500 μs time delay, indicating a concentration above ∼60 μmol/L. Importantly, however, Figure 4C shows that metabolic activity is inhibited upon the addition of an antimicrobial agent (potassium metabisulfite, PMB), and the O_2 concentration is brought back to baseline after 10 h of PMB exposure (shown in red and black).

CONCLUSIONS

In summary, our approach of integrating persistent luminescence nanoparticles into an optode-based nanosensor allowed for autofluorescence-free measurements in biological samples. The ion-selective optode approach offers the advantage of adjusting the dynamic range and selectivity based on the sensing components in the polymeric matrix.[15,24] As the ion-selective, persistent luminescence nanosensors all function on the same ion-exchange equilibrium, the selectivity was very easily modulated by varying only the ionophore. This modularity allowed us to develop persistent luminescence nanosensors for five different biologically relevant analytes by using $ZnGa_2O_4$:Cr^{3+} as the transducer. It is important to note that this feature would likely not be possible with other nonoptode-based sensor designs without rethinking how to incorporate the PLNPs into the sensor mechanism. While long-lifetime emissions have traditionally been utilized for O_2 quantification using phosphorescence lifetime imaging or custom microscope/CCD camera setups,[44,45] these systems are often costly or challenging to assemble for end users. Instead, we showed that ratiometric O_2 PLNs can be used in a standard plate reader for facile time-resolved monitoring of O_2 consumption in a high-throughput manner.[46] Overall, we envision a PLNP nanocomposite serving as a multifunctional and highly adaptable platform for autofluorescence-free sensing and imaging across a wide range of complex biological systems.

ASSOCIATED CONTENT

Supporting Information

The Supporting Information is available free of charge at https://pubs.acs.org/doi/10.1021/acssensors.4c00653.

Excitation spectrum of ZGO; calculation of the effective luminescence lifetime from the biphasic decay of ZGO; luminescence decay of ZGO; DLS and zeta measure-

https://doi.org/10.1021/acssensors.4c00653
ACS Sens. 2024, 9, 3307−3315

ments of ion PLNs, O_2 PLNs, and NCs; nanocomposites can overcome the autofluorescence of FBS; BB absorbance end point and spectra for respective ion PLNs; transmission electron micrographs of K^+ and O_2 PLNs; K^+ PLN midpoint response and hill slope are the same regardless of the time-gate; K^+ PLNs are reversible; K^+ PLN, Na^+ PLN, and Ca^{2+} PLN functional lifetimes; selectivity coefficients for all ion PLNs; ion PLN response to Hofmeister series without the incorporation of an ionophore; PLNs do not respond without BB or ionophore incorporation; absorbance spectra of pH PLNs in response to pHs 3−9; pH PLN midpoint response and hill slope are the same regardless of the time-gate; pH PLNs do not respond to K^+ or Na^+ (10 μM−100 mM); pH PLN functional lifetime; overcoming the inner filter effect; pH PLN calibration in FBS using IFE adjustment—variable delay times; pH PLN response in FBS without a time-gate; K^+ PLNs using ChII instead of blueberry; PdBP luminescence intensity as a function of O_2 with different delay times and ZGO luminescence intensity as a function of O_2 with different delay times; Stern−Volmer and pseudo-Stern−Volmer equations; PdTPTBP Stern−Volmer plot and time-gated calibrations; raw O_2 calculations for O_2 in the yeast assay; plate setup of yeast assay with O_2 PLNs; one-phase exponential decay equation used to calculate O_2 from ratiometric signals; best fit parameters from nonlinear regression of exponential decay; ratiometric signals for the yeast assay; calculated O_2 from the yeast assay; raw PdTPTBP signals from O_2 PLNs for the yeast assay with and without time-gate; raw ZGO signals for the yeast assay (from O_2 PLNs) with and without time-gate; ZGO signal in the yeast assay (from O_2 PLNs) without yeast control with and without time-gate; optical density data for the yeast assay (PDF)

AUTHOR INFORMATION

Corresponding Author

Kevin J. Cash − *Quantitative Biosciences and Engineering Program and Department of Chemical and Biological Engineering, Colorado School of Mines, Golden, Colorado 80401, United States;* orcid.org/0000-0002-9748-2530; Email: kcash@mines.edu

Authors

Tyler Z. Sodia − *Quantitative Biosciences and Engineering Program, Colorado School of Mines, Golden, Colorado 80401, United States;* orcid.org/0000-0002-3198-3340

Hanna L. Tetu − *Department of Chemistry, Colorado School of Mines, Golden, Colorado 80401, United States;* orcid.org/0000-0003-1357-8787

Samuel C. Saccomano − *Department of Chemical and Biological Engineering, Colorado School of Mines, Golden, Colorado 80401, United States;* orcid.org/0000-0001-9105-2663

Elizabeth G. Letch − *Quantitative Biosciences and Engineering Program, Colorado School of Mines, Golden, Colorado 80401, United States;* orcid.org/0009-0007-2303-072X

John M. Branning, Jr. − *Quantitative Biosciences and Engineering Program, Colorado School of Mines, Golden, Colorado 80401, United States; The MITRE Corporation, Bedford, Massachusetts 01730, United States;* orcid.org/0000-0003-3588-9033

Adrian A. Mendonsa − *Department of Chemical and Biological Engineering, Colorado School of Mines, Golden, Colorado 80401, United States;* orcid.org/0000-0002-6817-9778

Shubham Vyas − *Department of Chemistry, Colorado School of Mines, Golden, Colorado 80401, United States;* orcid.org/0000-0002-5849-8919

Complete contact information is available at: https://pubs.acs.org/10.1021/acssensors.4c00653

Author Contributions

Conceptualization: K.J.C. and T.Z.S.; methodology: K.J.C. and T.Z.S.; formal analysis: T.Z.S.; investigation: T.Z.S., S.C.S., E.G.L., J.M.B., and A.A.M.; data curation: T.Z.S., H.L.T., S.C.S., E.G.L., J.M.B., and A.A.M.; writing—original draft preparation: T.Z.S.; writing—review and editing: T.Z.S. and K.J.C.; visualization: T.Z.S. and A.A.M.; supervision: T.Z.S., K.J.C., and S.V.; project administration: K.J.C. and T.Z.S.; funding acquisition: K.J.C.

Funding

This material is based upon the work supported by the National Science Foundation under Grant No. 1944204.

Notes

The authors declare no competing financial interest.

[⊥]The author's affiliation with The MITRE Corporation is for identification purposes only and is not intended to convey or imply MITRE's concurrence with, or support for, the positions, opinions, or viewpoints expressed by the author. Approved for Public Release, Distribution Unlimited. Public Release Case Number 24-0224.

ACKNOWLEDGMENTS

We would like to thank Sara Russo, Adam Job, and Saeed Ahmadi Vaselabadi for their help with HR-TEM and XRD.

ABBREVIATIONS

PLNP, persistent luminescence nanoparticle; PLN, persistent luminescence nanosensor; ZGO:Cr^{3+}, chromium-doped zinc gallate; NP, nanoparticle; TMOS, trimethoxy(octyl)silane; BB, blueberry (blueberry-C6-ester-652); ChII, chromoionophore II; PdTPTBP, palladium tetraphenyl tetrabenzoporphine

REFERENCES

(1) Rong, G.; Tuttle, E. E.; Reilly, A. N.; Clark, H. A. Recent Developments in Nanosensors for Imaging Applications in Biological Systems. *Annu. Rev. Anal. Chem.* **2019**, *12* (1), 109−128.

(2) Doussineau, T.; Schulz, A.; Lapresta-Fernandez, A.; Moro, A.; Körsten, S.; Trupp, S.; Mohr, G. J. On the Design of Fluorescent Ratiometric Nanosensors. *Chem. - Eur. J.* **2010**, *16* (34), 10290−10299.

(3) Saccomano, S. C.; Jewell, M. P.; Cash, K. J. A Review of Chemosensors and Biosensors for Monitoring Biofilm Dynamics. *Sens. Actuators Rep.* **2021**, *3*, No. 100043.

(4) Wu, S.; Li, Y.; Ding, W.; Xu, L.; Ma, Y.; Zhang, L. Recent Advances of Persistent Luminescence Nanoparticles in Bioapplications. *Nano-Micro Lett.* **2020**, *12* (1), No. 70, DOI: 10.1007/s40820-020-0404-8.

(5) Sun, X.; Song, L.; Liu, N.; Shi, J.; Zhang, Y. Chromium-Doped Zinc Gallate Near-Infrared Persistent Luminescence Nanoparticles in Autofluorescence-Free Biosensing and Bioimaging: A Review. *ACS Appl. Nano Mater.* **2021**, *4* (7), 6497−6514.

(6) Shi, L.; Shao, J.; Jing, X.; Zheng, W.; Liu, H.; Zhao, Y. Autoluminescence-Free Dual Tumor Marker Biosensing by Persistent

Luminescence Nanostructures. *ACS Sustainable Chem. Eng.* **2020**, *8* (1), 686−694.
(7) Liu, J.-L.; Zhao, X.; Chen, L.-J.; Pan, L.-M.; Yan, X.-P. Dual-Emissive Persistent Luminescence Nanoparticle-Based Charge-Reversible Intelligent Nanoprobe for Persistent Luminescence-Ratio Bioimaging along with Chemo-Photothermal Synergic Therapy. *Anal. Chem.* **2021**, *93* (19), 7348−7354.
(8) Pan, L.-M.; Zhao, X.; Wei, X.; Chen, L.-J.; Wang, C.; Yan, X.-P. Ratiometric Luminescence Aptasensor Based on Dual-Emissive Persistent Luminescent Nanoparticles for Autofluorescence- and Exogenous Interference-Free Determination of Trace Aflatoxin B1 in Food Samples. *Anal. Chem.* **2022**, *94* (16), 6387−6393.
(9) Feng, F.; Chen, X.; Li, G.; Liang, S.; Hong, Z.; Wang, H.-F. Afterglow Resonance Energy Transfer Inhibition for Fibroblast Activation Protein-α Assay. *ACS Sens.* **2018**, *3* (9), 1846−1854.
(10) Wang, J.; Ma, Q.; Zheng, W.; Liu, H.; Yin, C.; Wang, F.; Chen, X.; Yuan, Q.; Tan, W. One-Dimensional Luminous Nanorods Featuring Tunable Persistent Luminescence for Autofluorescence-Free Biosensing. *ACS Nano* **2017**, *11* (8), 8185−8191.
(11) Luo, Q.; Wang, W.; Tan, J.; Yuan, Q. Surface Modified Persistent Luminescence Probes for Biosensing and Bioimaging: A Review. *Chin. J. Chem.* **2021**, *39* (4), 1009−1021.
(12) Paterson, A. S.; Raja, B.; Garvey, G.; Kolhatkar, A.; Hagström, A. E. V.; Kourentzi, K.; Lee, T. R.; Willson, R. C. Persistent Luminescence Strontium Aluminate Nanoparticles as Reporters in Lateral Flow Assays. *Anal. Chem.* **2014**, *86* (19), 9481−9488.
(13) Yin, Z.; Zhu, L.; Lv, Z.; Li, M.; Tang, D. Persistent Luminescence Nanorods-Based Autofluorescence-Free Biosensor for Prostate-Specific Antigen Detection. *Talanta* **2021**, *233*, No. 122563.
(14) Mistlberger, G.; Crespo, G. A.; Bakker, E. Ionophore-Based Optical Sensors. *Annu. Rev. Anal. Chem.* **2014**, *7* (1), 483−512.
(15) Du, X.; Xie, X. Ion-Selective Optodes: Alternative Approaches for Simplified Fabrication and Signaling. *Sens. Actuators, B* **2021**, *335*, No. 129368.
(16) Sodia, T. Z.; David, A. A.; Chesney, A. P.; Perri, J. N.; Gutierrez, G. E.; Nepple, C. M.; Isbell, S. M.; Cash, K. J. Nanoparticle-Based Liquid−Liquid Extraction for the Determination of Metal Ions. *ACS Sens.* **2021**, *6* (12), 4408−4416.
(17) Ruckh, T. T.; Skipwith, C. G.; Chang, W.; Senko, A. W.; Bulovic, V.; Anikeeva, P. O.; Clark, H. A. Ion-Switchable Quantum Dot Förster Resonance Energy Transfer Rates in Ratiometric Potassium Sensors. *ACS Nano* **2016**, *10* (4), 4020−4030.
(18) Xie, L.; Qin, Y.; Chen, H.-Y. Polymeric Optodes Based on Upconverting Nanorods for Fluorescent Measurements of PH and Metal Ions in Blood Samples. *Anal. Chem.* **2012**, *84* (4), 1969−1974.
(19) Ferris, M. S.; Chesney, A. P.; Ryan, B. J.; Ramesh, U.; Panthani, M. G.; Cash, K. J. Silicon Nanocrystals as Signal Transducers in Ionophore-Based Fluorescent Nanosensors. *Sens. Actuators, B* **2021**, *331*, No. 129350, DOI: 10.1016/j.snb.2020.129350.
(20) Galyean, A. A.; Behr, M. R.; Cash, K. J. Ionophore-Based Optical Nanosensors Incorporating Hydrophobic Carbon Dots and a PH-Sensitive Quencher Dye for Sodium Detection. *Analyst* **2018**, *143* (2), 458−465.
(21) Wang, R.; Du, X.; Wu, Y.; Zhai, J.; Xie, X. Graphene Quantum Dots Integrated in Ionophore-Based Fluorescent Nanosensors for Na + and K+. *ACS Sens.* **2018**, *3* (11), 2408−2414.
(22) Ferris, M. S.; Behr, M. R.; Cash, K. J. An Ionophore-Based Persistent Luminescent 'Glow Sensor' for Sodium Detection. *RSC Adv.* **2019**, *9* (56), 32821−32825.
(23) Li, Z.; Zhang, Y.; Wu, X.; Huang, L.; Li, D.; Fan, W.; Han, G. Direct Aqueous-Phase Synthesis of Sub-10 Nm "Luminous Pearls" with Enhanced in Vivo Renewable Near-Infrared Persistent Luminescence. *J. Am. Chem. Soc.* **2015**, *137* (16), 5304−5307.
(24) Ferris, M. S.; Katageri, A. G.; Gohring, G. M.; Cash, K. J. A Dual-Indicator Strategy for Controlling the Response of Ionophore-Based Optical Nanosensors. *Sens. Actuators, B* **2018**, *256*, 674−681.
(25) Saccomano, S. C.; Cash, K. J. A Near-Infrared Optical Nanosensor for Measuring Aerobic Respiration in Microbial Systems. *Analyst* **2021**, *147*, 120−129, DOI: 10.1039/D1AN01855H.
(26) Tien, T.; Saccomano, S. C.; Martin, P. A.; Armstrong, M. S.; Prud'homme, R. K.; Cash, K. J. Sensors in a Flash! Oxygen Nanosensors for Microbial Metabolic Monitoring Synthesized by Flash Nanoprecipitation. *ACS Sens.* **2022**, *7*, 2606−2614, DOI: 10.1021/acssensors.2c00859.
(27) Mendonsa, A. A.; Soeldner, C. C.; Mudd, N. E.; Saccomano, S. C.; Cash, K. J. Triplet−Triplet Annihilation Upconversion-Based Oxygen Sensors to Overcome the Limitation of Autofluorescence. *ACS Sens.* **2023**, *8* (8), 3043−3050.
(28) Lin, Q.; Li, Z.; Yuan, Q. Recent Advances in Autofluorescence-Free Biosensing and Bioimaging Based on Persistent Luminescence Nanoparticles. *Chin. Chem. Lett.* **2019**, *30* (9), 1547−1556.
(29) Saad, W. S.; Prud'homme, R. K. Principles of Nanoparticle Formation by Flash Nanoprecipitation. *Nano Today* **2016**, *11* (2), 212−227.
(30) Zacchia, M.; Abategiovanni, M. L.; Stratigis, S.; Capasso, G. Potassium: From Physiology to Clinical Implications. *Kidney Dis.* **2016**, *2* (2), 72−79.
(31) Robinson, K. J.; Soda, Y.; Bakker, E. Recent Improvements to the Selectivity of Extraction-Based Optical Ion Sensors. *Chem. Commun.* **2022**, *58* (27), 4279−4287.
(32) Bakker, E.; Bühlmann, P.; Pretsch, E. Carrier-Based Ion-Selective Electrodes and Bulk Optodes. 1. General Characteristics. *Chem. Rev.* **1997**, *97* (8), 3083−3132.
(33) Bühlmann, P.; Pretsch, E.; Bakker, E. Carrier-Based Ion-Selective Electrodes and Bulk Optodes. 2. Ionophores for Potentiometric and Optical Sensors. *Chem. Rev.* **1998**, *98* (4), 1593−1688.
(34) Fluorescence Sensing. In *BT - Principles of Fluorescence Spectroscopy*; Lakowicz, J. R., Ed.; Springer US: Boston, MA, 2006; pp 623−673.
(35) Sahari, A.; Ruckh, T. T.; Hutchings, R.; Clark, H. A. Development of an Optical Nanosensor Incorporating a PH-Sensitive Quencher Dye for Potassium Imaging. *Anal. Chem.* **2015**, *87* (21), 10684−10687.
(36) Xie, X.; Crespo, G. A.; Bakker, E. Oxazinoindolines as Fluorescent H+ Turn-On Chromoionophores For Optical and Electrochemical Ion Sensors. *Anal. Chem.* **2013**, *85* (15), 7434−7440.
(37) Xie, X.; Gutiérrez, A.; Trofimov, V.; Szilagyi, I.; Soldati, T.; Bakker, E. Charged Solvatochromic Dyes as Signal Transducers in PH Independent Fluorescent and Colorimetric Ion Selective Nanosensors. *Anal. Chem.* **2015**, *87* (19), 9954−9959.
(38) Xie, X.; Szilagyi, I.; Zhai, J.; Wang, L.; Bakker, E. Ion-Selective Optical Nanosensors Based on Solvatochromic Dyes of Different Lipophilicity: From Bulk Partitioning to Interfacial Accumulation. *ACS Sens.* **2016**, *1* (5), 516−520.
(39) Quaranta, M.; Borisov, S. M.; Klimant, I. Indicators for Optical Oxygen Sensors. *Bioanal. Rev.* **2012**, *4* (2), 115−157.
(40) Sodia, T. Z.; Cash, K. J. Editors' Choice—Luminescent Oxygen Sensors: Valuable Tools for Spatiotemporal Exploration of Metabolism in In Vitro Systems. *ECS Sens. Plus* **2023**, *2* (3), No. 032401.
(41) Jewell, M. P.; Galyean, A. A.; Harris, J. K.; Zemanick, E. T.; Cash, K. J. Luminescent Nanosensors for Ratiometric Monitoring of Three-Dimensional Oxygen Gradients in Laboratory and Clinical Pseudomonas Aeruginosa Biofilms. *Appl. Environ. Microbiol.* **2019**, *85* (20), No. e01116-19.
(42) Jewell, M. P.; Greer, M. D.; Dailey, A. L.; Cash, K. J. Triplet-Triplet Annihilation Upconversion Based Nanosensors for Fluorescence Detection of Potassium. *ACS Sens.* **2020**, *5* (2), 474−480.
(43) Zanetti, C.; Li, L.; Gaspar, R. D.; Santovito, E.; Elisseeva, S.; Collins, S. G.; Maguire, A. R.; Papkovsky, D. B. Susceptibility of the Different Oxygen-Sensing Probes to Interferences in Respirometric Bacterial Assays with Complex Media. *Sensors* **2024**, *24*, No. 267, DOI: 10.3390/s24010267.
(44) Koren, K.; Moßhammer, M.; Scholz, V. V.; Borisov, S. M.; Holst, G.; Kühl, M. Luminescence Lifetime Imaging of Chemical Sensors—A Comparison between Time-Domain and Frequency-Domain Based Camera Systems. *Anal. Chem.* **2019**, *91* (5), 3233−3238.

(45) Moßhammer, M.; Scholz, V. V.; Holst, G.; Kühl, M.; Koren, K. Luminescence Lifetime Imaging of O2 with a Frequency-Domain-Based Camera System. *J. Visualized Exp.* **2019**, No. 154, No. e60191, DOI: 10.3791/60191.

(46) Sodia, T. Z.; Tetu, H. L.; Saccomano, S. C.; Letch, E. G.; Branning, J. M., Jr.; Mendonsa, A. A.et al. Persistent Luminescence Nanosensors: A Generalized Optode-based Platform for Autofluorescence-free Sensing in Biological Systems *ChemRxiv*, 2024. (accessed May 10, 2024).

https://doi.org/10.1021/acssensors.4c00653
ACS Sens. 2024, 9, 3307−3315